

In-drop capillary spooling of spider capture thread inspires hybrid fibres with mixed solid-liquid mechanical properties

Hervé Eletro^{*}, Sébastien Neukirch^{*}, Fritz Vollrath[†] and Arnaud Antkowiak^{*}

^{*}Sorbonne Universités, UPMC Univ Paris 06, CNRS, UMR 7190 Institut Jean Le Rond d'Alembert, F-75005 Paris, France., and [†]Oxford Silk Group, Zoology Department, University of Oxford, UK

Submitted to Proceedings of the National Academy of Sciences of the United States of America

An essential element in the web-trap architecture, the capture silk spun by ecribellate orb spiders consists of glue droplets sitting astride a silk filament. Mechanically this thread presents a mixed solid/liquid behaviour unknown to date. Under extension, capture silk behaves as a particularly stretchy solid, owing to its molecular nanosprings, but it totally switches behaviour in compression to now become liquid-like: it shrinks with no apparent limit while exerting a constant tension. Here, we unravel the physics underpinning the unique behaviour of this "liquid wire" and demonstrate that its mechanical response originates in the shape-switching of the silk filament induced by buckling within the droplets. Learning from this natural example of geometry and mechanics, we manufactured novel programmable liquid wires that present novel pathways for the design of new hybrid solid-liquid materials.

Hybrids made of different materials often display effective properties far exceeding those of their components (1): zinc-coated steel is both strong and corrosion-resistant, metal foams (hybrids of metal and air) are stiff, light and crushable at the same time, making them perfect candidates to absorb energy in a car crash (2, 3). Nature also provides many exquisite examples of hybrid design such as the seashell nacre, both stiff and tough thanks to its inner 'brick-and-mortar' structure composed of rigid, though brittle, inclusions surrounded by a crack arresting soft organic matrix (4), or the bamboo stem with its hollow core and honeycomb-shaped cells that maximize the ratio of bending rigidity over weight (5). A most interesting natural hybrid material is the spider's capture thread, which consists of a core filament that supports glue droplets. Here we report on the arresting mechanical behaviour of this capture thread, that changes from solid-like in extension to liquid-like in compression. We trace this behaviour back to the core filament's buckling inside the droplets. A synthetic version of this natural system then allows us to copy the remarkable properties of spider's capture thread to a novel type of hybrid material.

Spiders use different kinds of silk to build their webs, and a typical ecribellate orb-web combines dry and smooth radial threads with wet and droplet-covered spiral threads (6, 7, 8, 9, 10). The adhesive nature of these droplets enables the spiral capture thread to perform its primary function of catching insect preys (6). Apart from being sticky, these capture threads also prove to be particularly resilient to tensile tests: extensive studies on their mechanical behaviour (11, 6) revealed that, when stretched, the thread elongates to three times its web-length without breaking and recoils back with no noticeable hysteresis or sagging when relaxed (12). This stretchiness confers spider silk a strength tenfold that of natural or synthetic rubber (13, 14). These remarkable extensional properties rely on the macromolecular architecture of capture silk (15, 16). The ability to cope with stretch is crucial for spider capture threads for it provides their unusually large toughness (energy required for rupture), which in turn allows them to absorb the kinetic energy of incident preys without breaking. Far less understood is the behaviour of the thread when compressed: unlike any solid fibre that sags or buckles, it keeps taut and self-adapts to compression. Figure 1 illustrates this singular behaviour, reminiscent of the response of liquid films to compression events: liquid films do not buckle upon squeezing, but rather self-adapt (17). And as for liquid films, self-adaptation for the capture thread is an indication for fibre self-tension. This liquid-like behaviour in compression suggests that more than merely endowing the web with adhesion, capture silk might well have the additional mechanical function of preserving the web structural integrity. Indeed, without self-adaptation, single sticky strands would touch during relaxation events and thereby irretrievably damage the web. With sagging suppressed, the sticky strands are secured apart.

Significance

The spiraling capture threads of spider orb webs are covered with thousands of tiny glue droplets whose primary function is to entrap insects. In this paper we demonstrate that the function of the drops goes beyond that of glueing preys for they also play a role in the mechanical properties of these fibres – usually ascribed solely to the complex molecular architecture of the silk. Indeed each of the droplets can spool and pack the core silk filament, thus keeping the thread and the whole web under tension. We demonstrate that this effect is the result of the interplay between elasticity and capillarity by making a fully artificial drops-on-fibre compound as extensible as capture thread is.

Reserved for Publication Footnotes

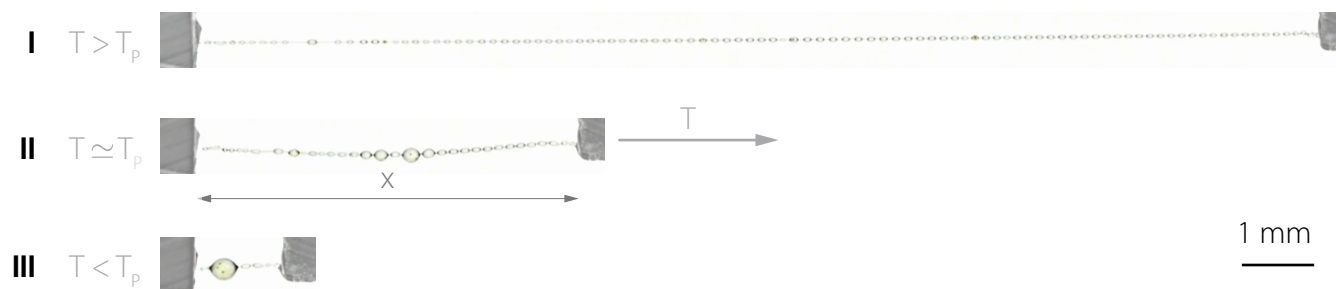


Figure 1. A liquid-like fibre. Whether stretched or relaxed, the typical capture silk thread of an araneid orb spider (here *Nephila edulis*) remains taut. Force monitoring reveals that when subjected to large tension T the fibre behaves like a spring (I). As T is decreased, a force plateau $T \approx T_p$ is reached, along which the thread adopts a wide range of lengths, just as soap films do (II). At lower tensions, $T < T_p$, the thread is totally contracted (III). See Supplementary Movie S4 for full cycle.

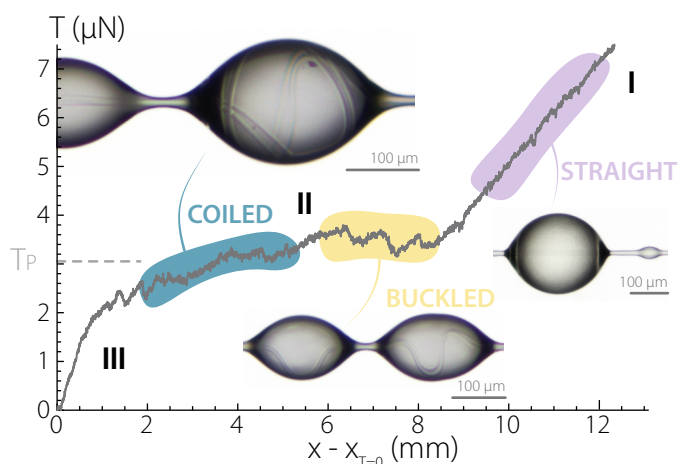


Figure 2. Shape-induced functionalization. Quasi-static force measurements on spider capture threads combined with microscopic observations reveal that the core filament coils into the droplets ($\sim 250\text{--}300\ \mu\text{m}$ wide) along a force plateau $T \sim T_p$ (liquid-like response). For larger forces $T > T_p$, the fibre straightens and a solid-like behaviour is recovered. The particular shape of this force-extension curve can be attributed to a shape-induced functionalization of the fibre by the glue droplets. See also Supplementary Movies S1 and S2.

In the present paper, we investigate and disentangle the mechanism underpinning the unique behaviour of spider capture silk. Based on these insights we design a mechanical hybrid that behaves as a solid when stretched, but as a liquid when compressed.

The spectacular macroscopic properties of hybrids often originate in a physical effect that occurs at the microstructural level (which needs not be molecular, see *e.g.* the buckling of the walls of a unit cell in a cellular solid (2, 18)). To investigate the physics of the mechanical hybrid character of spider capture thread, we performed mechanical tests on a single thread alongside microscopic observations of its microstructure. Figure 2 shows the relaxation of a freshly

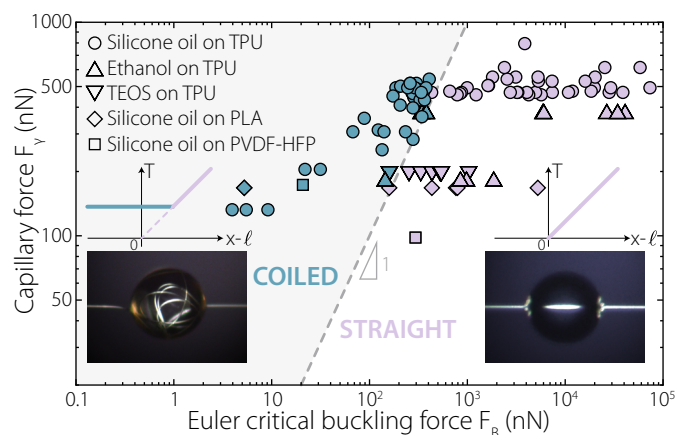


Figure 3. Spooling activation. In-drop spooling can also be achieved by synthetic fibres wet by droplets of various newtonian liquids. The phase diagram summarizes experiments performed with different materials and liquids in a quasi-static displacement-controlled setting. Each experiment consists in releasing the external tension on an initially taut system. Spooled or straight filament conformation are then observed within the droplets (blue or purple points respectively). These data demonstrate that the spooling threshold corresponds to a capillarity-induced buckling condition: spooling spontaneously occurs as soon as the capillary force exerted by the drop F_γ exceeds the Euler buckling load of the filament F_B . Note that, contrary to classic buckling, this spooling continues to proceed as long as the previous force condition is fulfilled, which suggests a subcritical nature for this elastocapillary instability. The composite overall mechanical response (sketched in insets) also sharply changes past the threshold to exhibit a liquid-like plateau force.

harvested biological sample. Starting from a stretched state (region I), the force-elongation curve shows that the thread behaves as a regular elastic solid undergoing relaxation: the monitored tension decreases almost linearly with the imposed displacement. In this regime, the capture thread adopts a classic drop-on-straight filament conformation, evocative of unduloidal-shaped drops sitting astride textile fibres (19), glass filaments (20), mammalian hairs (21), or feathers (22). But as relaxation proceeds further, the mechanical behaviour

of the capture thread switches from solid to liquid. This sudden change can be read directly from the mechanical testing: in region II, the recorded tension becomes virtually independent of the imposed displacement. This plateau tension is the typical signature of the response of liquid or soap films to tensile or compressive solicitations. Strikingly, this behavioural change coincides with a sharp modification of the micro-structure: while the overall composite remains taut, the core filament now buckles within each glue droplet. At even higher compressions, spools of slack filament form within the drops and keep on accumulating until eventually the overall tension falls (region III). Such spools have previously been observed in samples of post-mortem capture threads, but the physics underlying their formation, and in particular the potential roles of the filament molecular structure or of the glue viscoelasticity in this formation, has remained unclear so far (6).

The coincidence between the change in the mechanical responses of the capture thread at the global scale and the change in the conformations of the core filament at the drop scale is intriguing and requires further investigation. For so, let us consider a composite system consisting of a synthetic core filament and of a liquid droplet, and examine the link between the global mechanical response of the system and the local filament geometry. Specifically we investigate the possibility of a buckling-induced activation of the composite. Surface tension is known to promote buckling (23, 24), snapping (25), or wrinkling (26) of thin lamellar structures. In the drop-filament composite, and in absence of any external load, local buckling is initiated when the capillary force developed near each meniscus of a single drop $F_\gamma = 2\pi h\gamma \cos\theta$ exceeds the Euler buckling load $F_B = kEI/D^2$, where h , γ , θ , E , I , D , and k denote respectively the filament radius, the liquid-air surface tension, the contact angle of the liquid on the filament, the bending stiffness of the core filament, the wet length, and the Euler buckling factor. The h^4 scaling of the filament’s bending stiffness constitutes however a strong restriction for capillarity-induced buckling, typically limiting the manifestation of this phenomenon in filaments in the nm- μ m range – thereby supporting the observed in-drop buckling of micronic spider capture threads, while explaining why hairs of 80 μ m diameter do not buckle when wet, but rather simply clump (27). This fully mechanical scenario, involving capillarity and elasticity as only ingredients, suggests that any drop sitting astride any filament could make it buckle, provided the force condition $F_\gamma > F_B$ is satisfied. To test this hypothesis, we conducted extensive experiments with various Newtonian liquid drops surrounding synthetic (*i.e.* non-biological) filaments of different diameters and made of diverse materials. Upon release of external tension, we found in-drop elastocapillary buckling to be indeed activated as soon as the capillary force overcomes the Euler buckling load, irrespective of the materials involved, see Fig. 3 and Supplementary Movie S5. Note that we have here used the value $k = \pi^2$ for the Euler buckling factor, expressing the fact that the fibre can freely rotate at the meniscii (simply supported buckling), see (28). Contrary to conventional buckling, past the elastic instability threshold the core filament is not gently deformed but literally spooled and packed within the droplets, although the applied capillary force is constant. This behaviour, along with the localization of the bending deformation, are typical signatures of a subcritical instability. Furthermore, the global mechanical response of the composite changes instantly as soon as buckling is initiated at the drop scale: under large stretching, the composite behaviour is that of the core filament, but switches to that of a liquid film when compressed past the threshold

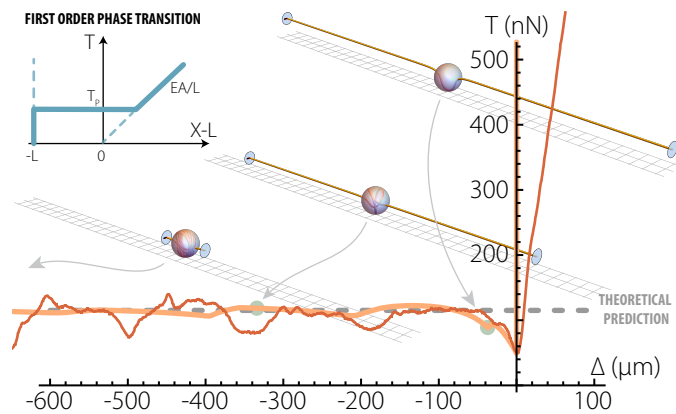


Figure 4. Structural phase transition and detailed mechanical response. Comparison between nano-Newton-resolved measurements on a composite polyurethane filament/silicone oil thread (red line), detailed simulations of an Elastica interacting with a droplet (orange line) and the first-order phase transition model (dashed grey line, full behavior also sketched in inset). Experiments were performed with a drop of wet length $D = 62 \pm 2\mu\text{m}$ and a filament of radius $h = 1 \pm 0.2\mu\text{m}$ and Young modulus $E = 17 \pm 3\text{MPa}$. Numerical equilibria are here followed with a continuation procedure, with $F_\gamma = 35EI/D^2$ and $L = 20D$. The plateau tension T_P given by the phase transition model (2) is here 115 nN. Beyond the nice overall agreement, the results reveal a difference between the buckling threshold and the plateau tension. This difference points to the subcritical nature of elastocapillary buckling, also evidenced by the sudden localisation of the filament visible in the insets. The numerical simulations allow to capture the fine details in the micro-mechanical response observed in the experiments, resulting in inhomogeneities in the Maxwell plateau. Sensor drift forced us to adjust the reference level for the experimental measurements, but the level difference between buckling threshold and plateau tension is well recovered. See also Supplementary Movies S3 and S5.

(see also Supplementary Movie S3). Thus the droplets have the double role of storing the excess thread and putting the whole composite in a state of tension. This behaviour is all the more arresting because real liquid cylinders instantaneously disintegrate due to Rayleigh-Plateau instability, making the liquid-like response of the composite truly unusual (see Supplementary Movie S1 for an illustration of the composite in action).

The geometry of slender elastic objects is known to control their mechanical response (29, 30). The composite under study here is no exception and we now explain how the in-drop filament geometry leads the thread to inherit the solid core filament mechanical properties when stretched, but the liquid drop properties when compressed. To shed light on this connection between the micro-structure and the global mechanical response, we consider a simple model where a bendable and stretchable elastic filament supports a liquid drop, the overall system now being subjected to an external tension T . Elastocapillary spooling activation can be described as a phase transition between a wet and coiled phase – where the filament is entirely packed within the liquid drop – and a dry and extended phase – where the filament runs straight outside the drop. The extended phase is characterized by a stretching modulus EA and a rest length ℓ_e . Under an applied tension, its extension is $x_e = (1 + \epsilon_e)\ell_e$, where ϵ_e is the extensional strain. The strain energy of the phase is then $\frac{1}{2}\ell_e EA\epsilon_e^2$, to which we add the solid-air interface energy $2\pi h\gamma_{sv}\ell_e$. The coiled phase is made up of the drop and the spooled filament inside the drop. The spools certainly adopt a complicated shape and the bending energy of the filament is $\frac{1}{2}EI \int_0^{\ell_c} \kappa(s)^2 ds$ where κ is the curvature of the filament and $I = \pi h^4/4$. Approximating the drop as spheri-

cal and the spools as arcs of circle, we write $\kappa = 2/D$ where D is the diameter of the drop. The bending energy is then $2\ell_c EI/D^2$. We note that in this approximation the extension of the phase $x_c = D$ is constant. We add the solid-liquid interface energy $2\pi h\gamma_{sl}\ell_c$ (the liquid-air interface energy, a constant, is not included) to obtain the total energy of the system $V = (\frac{1}{2}EA\epsilon_e^2 + 2\pi h\gamma_{sv})\ell_e + (2EI/D^2 + 2\pi h\gamma_{sl})\ell_c$. We replace ℓ_c and, discarding constant terms, re-write the total energy as $V = (\frac{1}{2}EA\epsilon_e^2 - 2EI/D^2 + 2\pi h\gamma \cos\theta)\ell_e$. Note that we have used Young-Dupré wetting relation $\gamma_{sv} - \gamma_{sl} = \gamma \cos\theta$, where θ is the liquid contact angle on the filament and γ the liquid-air interface energy per area. We note that the latent energy cost per unit length $\epsilon_0 = 2\pi h\gamma \cos\theta - \pi E h^4/2D^2$ involved in the transformation from the coiled to the extended phase is a typical signature of a first-order phase transition problem. From this expression we readily obtain a condition for spooling to be sustained. Indeed, for the coiled phase to be stable at small forces ϵ_0 has to be positive. This condition can be recast into a condition for the radius, where we recover the fact that only thin filaments exhibit in-drop spooling:

$$h < (4\gamma \cos\theta)^{1/3} E^{-1/3} D^{2/3} \quad [1]$$

Introducing the ratio $\rho = \ell_e/\ell$, we minimize V under the constraints of fixed extension $x = x_c + x_e$, and bounded ratio $0 \leq \rho \leq 1$. In the limit where $D \ll \ell$ and $\epsilon_0 \ll EA$, we find that the system can be entirely in the coiled phase ($\rho = 0$; filament fully packed in the drop) with tension $0 < T < \epsilon_0$, or entirely in the extended phase ($\rho = 1$) with tension $T = EA(x/\ell - 1) > \epsilon_0$. A third interesting possibility consists in a mixture of phases $0 < \rho < 1$. In this latter case, part of the filament is packed in the drop while the outer part is taut, consistent with our observations. As ρ is changed, the tension remains constant to a plateau value $T = T_P = \epsilon_0$, with

$$T_P = 2\pi h\gamma \cos\theta - \pi E h^4/2D^2 \quad [2]$$

To further explore the mechanical response of the composite system, we also performed detailed numerical computations of equilibrium of an inextensible and flexible elastic filament (29, 31, 28). The filament, held at both extremities with imposed distance x , is subjected to attracting meniscus forces F_γ at entrance and exit of a confining sphere. The loading (x, T) diagram, shown in Fig. 4, reveals inhomogeneities in the Maxwell line (32). These inhomogeneities are due to fine details in the micro-mechanical response of the system. Setting $F_\gamma = 2\pi h\gamma \cos\theta$, we plot in Fig. 4 the phase transition prediction given by Eq. (2), and we observe a nice agreement not only with the numerical computations, but also with nano-Newton-resolved mechanical testing of synthetic composites (here made of polyurethane filament and silicone oil droplet). We also note that both experiments and numerical simulations exhibit a kink between the two regimes that reveals a difference between the buckling threshold and the plateau tension, as already anticipated by our simple models and by the subcritical nature of the spooling (Fig. 3).

Unraveling the mechanics of spider capture silk allowed us to design a new type of fully self-assembling hybrid material with unprecedented mechanical function, switching from solid-like in extension to liquid-like in compression. This bioinspired hybrid can be manufactured with virtually any material, and provides novel functionalities such as fibre spooling or unspooling at the micron level, or constant force application for a wide range of extension while preserving tautness and reversibility. Strikingly, rather than being a failure threshold, buckling in this case proves to be a necessary condition for material activation.

Materials and Methods

Capture silk samples. Our *Nephila edulis* spider was kept in a $80 \times 80 \times 30$ cm vivarium, consisting of wood panels, PMMA windows and artificial plants. The spider was kept at high humidity (above 70%) and comfortable temperature (above 22°C) with a 12/12 hr day/night schedule. The spider was fed crickets and flies three times a week. Sections of web were carefully excised using a soldering iron for transfer within a rigid frame. To visualise the filament running through each droplet, the humidity was set to 100% rH for 15 minutes before observation. The humidity was then stepped down to 50% (observation) rH.

Artificial samples. PolyUrethane (TPU, Elastollan 1185A from BASF[®], Young's modulus $E = 17$ MPa) granules were deposited on a hot plate at 230°C . After melting, we used a tweezer to pick up a small droplet which was then stretched quickly while at the same time being released into ambient room temperature. This resulted in the creation of micron-sized, metre-long, soft filaments. The filament was then deposited on the measuring setup as outlined below. A droplet of silicone oil (Rhodorsil[®] 47V1000, surface tension $\gamma = 21.1\text{mN.m}^{-1}$) was then deposited by gently touching and brushing the filament with a drop hanging from a pipette. PLA (PolyLactic Acid, Young's modulus $E \sim 4$ GPa in the glassy and ~ 4 MPa in the rubbery state) filaments were processed the same way. PVDF-HFP samples were obtained by electrospinning. A droplet of PVDF-HFP (Young's modulus $E \sim 10$ MPa) in THF was electrospun at 12kV using a charged syringe tip, at room temperature and relative humidity. We thus obtain polymer cables made of many microfibers. The distribution of fibers radii and corresponding cable bending rigidity is inferred optically using a Leica microscope. We measured contact angles by superimposing optical images of drops on fibers to corresponding calculated profiles, and found $\theta_Y = 23^\circ \pm 2^\circ$ for TPU/silicone oil, $\theta_Y = 19^\circ \pm 2^\circ$ for TPU/ethanol, $\theta_Y = 31^\circ \pm 2^\circ$ for TPU/TEOS, $\theta_Y = 35^\circ \pm 2^\circ$ for PLA/silicone oil and $\theta_Y = 29^\circ \pm 2^\circ$ for PVDF-HFP/silicone oil. The surface tension of the liquid-air interface was measured to be $\gamma = 22.1\text{mN.m}^{-1}$ for ethanol, and $\gamma = 23.5\text{mN.m}^{-1}$ for TEOS. **Measurement methods.** Filament samples were transferred to the measuring setup by coiling one end around the tip of a FemtoTools FT-FS1000 (FT-FS100) capacitive deflection force sensor with range 50 nN-1mN (5 nN-100 μN) and gluing the other end to a glass slide as base. The force sensor was mounted on a linear micro positioner SmarAct SLC-1730 (repeatability 0.5 μm) and measurements are performed through a work station by USB connection. All the tests were performed in stretching at a speed of 25 $\mu\text{m/s}$, and considering the centimeter size in length of the sample, they can be considered to be quasi-static. The optical setup consisted of a Leica microscope (VZ85RC) mounted on a micro-step motor and a 3 megapixels Leica DFC-295 camera (400 \times zoom, 334 nm/pixel picture resolution) or a D800E Nikon camera with 3 10mm C-mount extension rings (937 nm/pixel video resolution and 374 nm/pixel photo resolution) alternatively. We used a Phlox 50x50 mm backlight, at 60000 lux or alternatively an optical fibre with LED lamp (Moritex MHF-M1002) with circular polarizer. Side views were acquired with a second D800E camera, with a 70mm extension tube and a 100mm macro Zeiss lens (7,27 microns/pixel video resolution). The force sensor was tared to zero with the fibre compressed slightly more than its slack length, so that it sags, but only minutely, be it for fibres with or without droplet. The measurement of the slack length was performed by pulling on the filament at one end by a few micrometers to straighten the fibre.

The TPU fibre diameter measurement was performed using Fiji software. A high-resolution picture of the fibre is analysed using the following steps : the contrast is enhanced up to the point that 0.4% of the pixels are saturated, then the grey value of the pixels on a line perpendicular to the fibre axis is plotted. The typical curve obtained this way resembles a downward pointing gaussian, thus the diameter of the fibre is extracted as the full width at half minimum of the peak.

Numerical computations. The windlass system is modeled as an elastic filament, obeying Kirchhoff equilibrium equations, in interaction with a sphere. Except at the two 'meniscus' points, the filament is prevented from touching or crossing the sphere through a soft-wall barrier potential. The equilibrium of the system is solved using two-points boundary-value problem techniques (shooting method in Mathematica, and collocation method using the Fortran - AUTO code).

ACKNOWLEDGMENTS. The present work was supported by ANR grants ANR-09-JCJC-0022-01 and ANR-14-CE07-0023-01, 'La Ville de Paris - Programme Émergence', Royal Society International Exchanges Scheme 2013/R1 grant IE130506, and the PEPS PTI program from CNRS. Support from the European Research Council (SP2-GA-2008-233409) and the US-AFOSR (FA9550-12-1-0294) is also acknowledged. We thank Régis Wunenburger for discussions and experimental advices on thread visualization within droplets, Christine Rollard for advices in spider housing and Natacha Krins for electrospinning the PVDF-HFP filaments. We also acknowledge Yves Bréchet for an enlightening discussion on hybrid materials.

References

1. M.F. Ashby and Y.J.M. Bréchet. Designing hybrid materials. *Acta Materialia*, 51(19):5801 – 5821, 2003.
2. Lorna J Gibson and Michael F Ashby. *Cellular solids: structure and properties*. Cambridge University Press, 1997.
3. John Banhart and Denis Weaire. On the road again: Metal foams find favor. *Physics Today*, 55(7):37–42, 2002.
4. John W.C. Dunlop and Peter Fratzl. Biological composites. *Annual Review of Materials Research*, 40(1):1–24, 2010.
5. Ulrike G. K. Wegst, Hao Bai, Eduardo Saiz, Antoni P. Tomsia, and Robert O. Ritchie. Bioinspired structural materials. *Nature Materials*, 14(1):23–36, 2015.
6. Rainer Foelix. *Biology of spiders*. Oxford University Press, 2010.
7. Brent D. Opell and Jason E. Bond. Changes in the mechanical properties of capture threads and the evolution of modern orb-weaving spiders. *Evolutionary Ecology Research*, 3(5):507–519, 2001.
8. Fritz Vollrath. Spider silk: Thousands of nano-filaments and dollops of sticky glue. *Current Biology*, 16(21):R925 – R927, 2006.
9. Brent D. Opell, Brian J. Markley, Charles D. Hannum, and Mary L. Hendricks. The contribution of axial fiber extensibility to the adhesion of viscous capture threads spun by orb-weaving spiders. *Journal of Experimental Biology*, 211(14):2243–2251, 2008.
10. Todd A. Blackledge, Nikolaj Scharff, Jonathan A. Codrington, Tamas Szüts, John W. Wenzel, Cheryl Y. Hayashi, and Ingi Agnarsson. Reconstructing web evolution and spider diversification in the molecular era. *Proceedings of the National Academy of Sciences*, 106(13):5229–5234, 2009.
11. Mark Denny. The physical properties of spider’s silk and their role in the design of orb-webs. *The Journal of Experimental Biology*, 65(2):483–506, 1976.
12. Fritz Vollrath and Donald T. Edmonds. Modulation of the mechanical properties of spider silk by coating with water. *Nature*, 340:305–307, 1989.
13. John M. Gosline, Mark W. Denny, and M. Edwin DeMont. Spider silk as rubber. *Nature*, 309(5968):551–552, 1984.
14. J.M. Gosline, P.A. Guerette, C.S. Ortlepp, and K.N. Savage. The mechanical design of spider silks: from fibroin sequence to mechanical function. *Journal of Experimental Biology*, 202(23):3295–3303, 1999.
15. Nathan Becker, Emin Oroudjev, Stephanie Mutz, Jason P. Cleveland, Paul K. Hansma, Cheryl Y. Hayashi, Dmitrii E. Makarov, and Helen G. Hansma. Molecular nanosprings in spider capture-silk threads. *Nature Materials*, 2(4):278–283, 2003.
16. Todd A. Blackledge, Adam P. Summers, and Cheryl Y. Hayashi. Gumfooted lines in black widow cobwebs and the mechanical properties of spider capture silk. *Zoology*, 108(1):41–46, 2005.
17. P.G. de Gennes, F. Brochard-Wyart, and D. Quéré. *Capillarity and Wetting Phenomena: Drops, Bubbles, Pearls, Waves*. Springer, 2003.
18. K. Bertoldi, P. M. Reis, S. Willshaw, and T. Mullin. Negative poisson’s ratio behavior induced by an elastic instability. *Advanced Materials*, 22(3):361–366, 2010.
19. N. K. Adam. Detergent action and its relation to wetting and emulsification. *Journal of the Society of Dyers and Colourists*, 53(4):121–129, 1937.
20. David Quéré. Fluid coating on a fiber. *Annual Review of Fluid Mechanics*, 31(1):347–384, 1999.
21. Brendan Joseph Carroll. Droplet formation and contact angles of liquids on mammalian hair fibres. *Journal of the Chemical Society, Faraday Transactions 1: Physical Chemistry in Condensed Phases*, 85(11):3853–3860, 1989.
22. C. Duprat, S. Protiere, A. Y. Beebe, and H. A. Stone. Wetting of flexible fibre arrays. *Nature*, 482(7386):510–513, 2012.
23. Sébastien Neukirch, Benoît Roman, Benoît de Gaude- maris, and José Bico. Piercing a liquid surface with an elastic rod: Buckling under capillary forces. *Journal of the Mechanics and Physics of Solids*, 55(6):1212–1235, 2007.
24. B. Roman and J. Bico. Elasto-capillarity: deforming an elastic structure with a liquid droplet. *Journal of Physics: Condensed Matter*, 22(49):493101, 2010.
25. Aurélie Fargette, Sébastien Neukirch, and Arnaud Antkowiak. Elastocapillary snapping: Capillarity induces snap-through instabilities in small elastic beams. *Phys. Rev. Lett.*, 112:137802, 2014.
26. Jiangshui Huang, Megan Juskiewicz, Wim H. de Jeu, Enrique Cerda, Todd Emrick, Narayanan Menon, and Thomas P. Russell. Capillary wrinkling of floating thin polymer films. *Science*, 317(5838):650–653, 2007.
27. J. Bico, B. Roman, L. Moulin, and A. Boudaoud. Adhesion: Elastocapillary coalescence in wet hair. *Nature*, 432(7018):690–690, 2004.
28. Hervé Elettro, Fritz Vollrath, Arnaud Antkowiak, and Sébastien Neukirch. Coiling of an elastic beam inside a disk: A model for spider-capture silk. *International Journal of Non-Linear Mechanics*, 75:59 – 66, 2015.
29. Basile Audoly and Yves Pomeau. *Elasticity and Geometry: From hair curls to the non-linear response of shells*. Oxford University Press, 2010.
30. A. Lazarus, H. C. B. Florijn, and P. M. Reis. Geometry-induced rigidity in nonspherical pressurized elastic shells. *Phys. Rev. Lett.*, 109:144301, 2012.
31. A. Antkowiak, B. Audoly, C. Josserand, S. Neukirch, and M. Rivetti. Instant fabrication and selection of folded structures using drop impact. *Proc. Natl Acad. Sci. U.S.A.*, 108(26):10400–10404, 2011.
32. James Clerk Maxwell. On the dynamical evidence of the molecular constitution of bodies. *Nature*, 11:357–359, 1875.